Physical Biology

PAPER

A biomechanical model for cell polarization and intercalation during *Drosophila* germband extension

RECEIVED
26 April 2015

REVISED
25 July 2015

ACCEPTED FOR PUBLICATION
13 August 2015

PUBLISHED
10 September 2015

Haihan Lan[1], **Qiming Wang**[2], **Rodrigo Fernandez-Gonzalez**[3,4] **and James J Feng**[5,6,7]

[1] Department of Electrical and Computer Engineering, University of British Columbia, Vancouver, BC V6T 1Z2, Canada
[2] Department of Mathematics and Statistics, York University, Toronto, ON M3J 1P3, Canada
[3] Institute of Biomaterials & Biomedical Engineering, University of Toronto, Toronto, ON M5S 3G9, Canada
[4] Department of Cell & Systems Biology, University of Toronto, Toronto, ON M5S 3G5, Canada
[5] Department of Mathematics, University of British Columbia, Vancouver, BC V6T 1Z2, Canada
[6] Department of Chemical and Biological Engineering, University of British Columbia, Vancouver, BC V6T 1Z3, Canada
[7] Author to whom any correspondence should be addressed.

E-mail: james.feng@ubc.ca

Keywords: cell intercalation, vertex model, myosin contraction, T1 transition

Supplementary material for this article is available online

Abstract

Germband extension during *Drosophila* development features the merging of cells along the dorsal–ventral (DV) axis and their separation along the anterior–posterior (AP) axis. This intercalation process involves planar cell polarity, anisotropic contractile forces along cell edges, and concerted cell deformation and movement. Although prior experiments have probed each of these factors separately, the connection among them remains unclear. This paper presents a chemo-mechanical model that integrates the three factors into a coherent framework. The model predicts the polarization of Rho-kinase, myosin and Bazooka downstream of an anisotropic Shroom distribution. In particular, myosin accumulates on cell edges along the DV axis, causing them to contract into a vertex. Subsequently, medial myosin in the cells anterior and posterior to the vertex helps to elongate it into a new edge parallel to the body axis. Thus, the tissue extends along the AP axis and narrows in the transverse direction through neighbor exchange. Model predictions of the polarity of the proteins and cell and tissue deformation are in good agreement with experimental observations.

1. Introduction

Axis elongation is a conserved morphogenetic process in which the head-to-tail or anterior–posterior (AP) axis of an animal is established. In the fruit fly *Drosophila melanogaster*, axis elongation occurs through the extension of an epithelial monolayer known as the germband. Cell intercalation is a central process in germband extension (GBE) [1, 2], although cell deformation and division also contribute [3, 4]. Mechanically, the intercalation process can be divided into two stages (figure 1): the shrinkage of the AP cell border into a vertex and the formation and elongation of a new dorsal–ventral (DV) border between the new neighbors. This sequence of events is often called the T1 process, borrowing from the terminology of foam rheology [5]. The T1 process involves neighbor swap among 4 cells. A similar process involving 5 to 11 cells, through the formation and resolution of the so-called rosette, has also been reported [6–8]. Although rosettes appear to be more prevalent and efficient in producing convergent-extension [6], they involve coordinated multi-cell behavior over longer range that is more complex than the T1 transition. For simplicity, we will focus this study on the T1 process.

Cell intercalation depends on the intricate interplay between the polarization of several signaling proteins on the one hand, and mechanical forces and deformation on the other [9–11]. Planar cell polarity (PCP) is a necessary precursor for intercalation. Blankenship *et al* [6, 7] found that the onset of PCP is signaled by F-actin enrichment on AP borders (figure 2). Then the kinase Rho-kinase (Rok) and the molecular motor non-muscle myosin-II localize on the AP borders, while Bazooka/PAR-3 (Baz) and E-cadherin localize along the DV borders. Polarized myosin contributes to the contraction of AP edges into vertices, which subsequently elongate into DV edges that

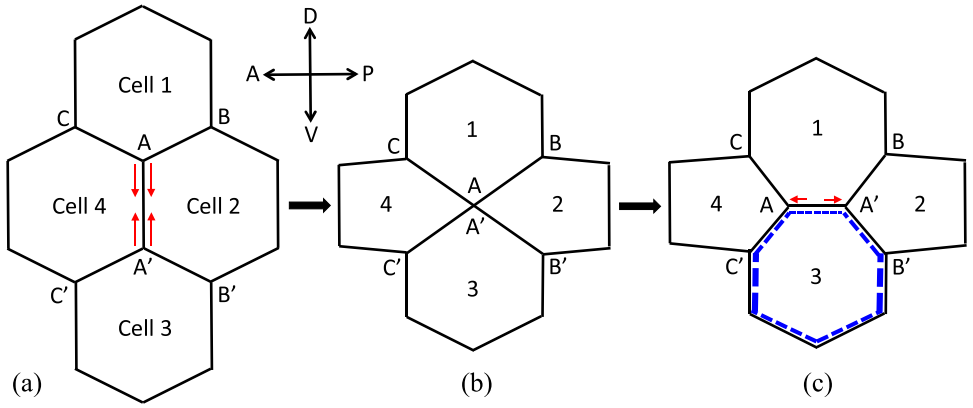

Figure 1. Schematic of cell intercalation through the T1 process. The anterior of the embryo is to the left and the posterior to the right; the dorsal side is up and the ventral side down (see inset; same convention hereafter). The vertical edge AA′ in (a) contracts into a vertex in (b), which then extends horizontally into a new edge AA′ in (c). In cell 3, the dash lines indicate the level of Shroom by their thickness, with the highest along the vertical edges and the lowest along the DV edge AA′. Following the literature [6, 8], we define the AP borders as the vertical borders separating two neighbors aligned in the AP direction, and the DV borders as horizontal.

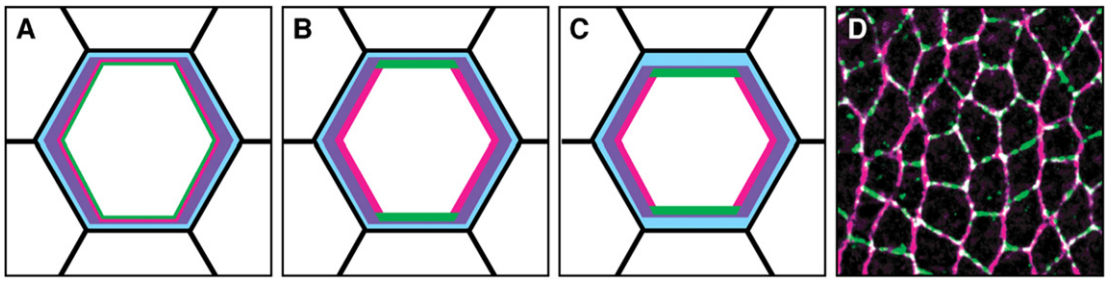

Figure 2. Illustration of the developing planar polarity in the germband. First, F-actin (purple) accumulates on AP edges (A). Then myosin (red) and Bazooka (green) localize onto the AP and DV edges, respectively, producing the polarized distribution in (B). Finally, E-cadherin (light blue) becomes enriched at DV edges (C). The confocal micrograph in (D) shows the exclusive localization of myosin and Bazooka corresponding to (B). Adapted from Zallen and Blakenship [7] with permission, © Elsevier Inc.

recruit E-cadherin and Baz. What is remarkable about these observations is the apparent antagonism between Rok and myosin on the one hand, and Baz and E-cadherin on the other. These are targeted to complementary cortical domains [6, 12, 13]. More recently, Simões *et al* [14] reported prominent roles of Rho-GTPase and Shroom in regulating the polarization of Rok and myosin prior to cell intercalation. Rho-GTPase, a well-known regulator of PCP and myosin contraction, localizes Rok to adherens junctions (AJs) along AP borders, but only induces partial Rok polarity. Meanwhile, Shroom is polarized by Rho, and acts 'to amplify and maintain Rho-kinase and myosin planar polarity and junctional localization' [14]. These observations provide a plausible scenario for the development of PCP prior to cell intercalation.

For the mechanics of AP border contraction, two mechanisms have been proposed so far, one focusing on the role of junctional myosin, the other on medial myosin. The junctional accumulation of myosin II along AP borders has been well documented [2, 8, 13]. Furthermore, myosin dynamics are regulated by tension in the AP edge through a *positive feedback loop* [8, 12]. The tensile load suppresses the dissociation of myosin from actin filaments, while accumulation of myosin will generate greater tension in turn. This suggests an explanation for the rising tension leading to contraction of the AP borders, and even the multi-cell borders prior to rosette formation [6, 7, 9]. In an alternative proposal, Lecuit *et al* [15–17] argued that the medial actomyosin network causes contraction of the AP border, while the junctional myosin plays a secondary role in stabilizing the contraction. Moreover, the medial *actomyosin flow*, driven by alternating polarity in E-cadherin [18], delivers the medial actomyosin network to the AP edges in pulses. At present, it is not clear which proposal more closely captures the true mechanism for AP edge contraction. Quite possibly both are at work.

The second stage of intercalation, resolution of the vertex and formation of the new DV edge, is even less well understood than the first. Blankenship *et al* [6] observed early F-actin and E-cadherin accumulation on the nascent DV borders, followed by enrichment of Bazooka several minutes later as the border elongates. Two factors may be implicated in DV border elongation. First, the contact between the two new neighbors (marked 1 and 3 in figure 1(c)) promotes E-cadherin

clustering and formation of new AJs, as in other scenarios of cell–cell adhesion [19]. Second, the new DV border may lengthen under active tension from its neighbors anterior and posterior to the DV border (e.g. cells marked 2 and 4 in figure 1(c)). Such tension may arise from junctional myosin on the two 'shoulders' (e.g. the boundaries between cells 1 and 2; 2 and 3 in figure 1(c)), or medial myosin in the neighbors, or even both. For lack of data, it is difficult to be more precise than such speculations at present.

To sum up the brief literature review, cell intercalation during *Drosophila* GBE is a complex process with two key components: polarity of signaling proteins and mechanical forces. Each has been examined separately in experimental studies, which have yielded important insights, e.g., on the complementary localization of Rok and Baz on the apical surface [12], and on the forces on AP and DV borders [2, 6, 8, 14, 15]. However, there is not yet an integral model that couples the biochemical and mechanical components together into a coherent framework. As far as we are aware, Rauzi *et al* [20] have presented the most comprehensive model for intercalation up to date. Similar to other vertex-based modeling [21, 22], this essentially amounts to the relaxation of an elastic network toward a state of minimum energy under prescribed forcing. Specifically, anisotropic line tension and cortical tension are imposed on different cell edges according to their orientation [20]. Thus, AP borders shrink and DV borders elongate. But how does this anisotropy in force arise from the polarization of signal proteins? How do the forces induce anisotropic contraction and elongation? Can one predict experimental data quantitatively based on the best estimation of parameters? What are the separate roles of junctional and medial myosin? These are the questions that have motivated the current study. Our goal is to assemble the existing experimental observations and hypotheses into a biomechanical model that is capable of predicting the polarization and mechanical deformation of the T1 process.

2. Model description

Our minimalist model strives for a balance between faithfulness and simplicity. We model four cells on a two-dimensional (2D) plane, the minimum required for realizing the T1 neighbor-exchange transition (figure 1). The two-dimensionality is because the germband is a monolayer of cells with their actomyosin network and AJs concentrated within a 1 μm apical band [22]. It is tempting to imagine the four-cell assembly as a 'periodic unit' representing the entire germband. But such an interpretation is invalid. First, GBE does not show spatial periodicity but a great deal of spatial heterogeneity and temporal stochasticity [6, 7]. Second, a high percentage of the cells form rosettes during GBE [6], which are not considered in the current model. Finally, imposing 2D periodicity in the model would preclude tissue-scale convergent-extension, as global cell movement and tissue contraction would violate the periodicity.

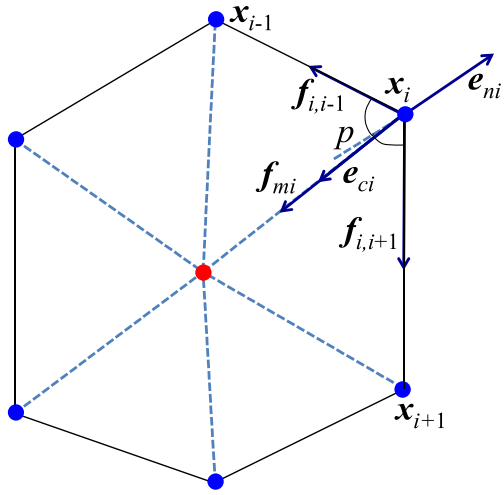

Figure 3. A cell is represented by six edges (solid lines) and six spokes (dashed lines). The various vectors depict the forces and unit vectors in equation (7); $\boldsymbol{e}_{ci}$ is the unit vector pointing from node i to the centroid, on which the medial myosin force acts, whereas $\boldsymbol{e}_{ni}$ is the unit normal vector that bisects the angle at node i, along which the pressure acts.

In reality, the four-cell assembly would interact with neighboring cells in a highly anisotropic and time-dependent fashion. It is difficult to include such interactions in the current framework. An attempt of using elastic springs to connect the peripheral nodes to a fixed outer boundary proved ineffective; details can be found in the supplementary material. Thus, we have adopted two measures to partially compensate for omitting the surrounding cells. First, we halve the forces on all the peripheral, 'free edges'. Interior, shared edges represent two membranes fused together, each with its underlying cortex. Peripheral edges consist of one membrane only. Besides, these edges are detached from the surrounding tissue and are thus less hindered in their movement and deformation. Second, we use the elastic modulus of all the edges as an adjustable parameter. As explained in the supplementary material, a larger modulus offers greater resistance to cell contraction and movement, which may stand in for the hindrance due to the surrounding tissue that is absent from our model.

As in other vertex models [22, 23], each cell is initially a hexagon, with 6 vertices and 6 cell borders or edges (figure 3). The borders of each cell possess passive elasticity due to the actin cortex and the AJs that bind the two membranes. In addition, junctional myosin also generates an active contractile force along the edges. The shared edge between neighboring cells is treated as a single entity. Besides, within each cell six spokes connect the vertices to a centroid. They represent actin cables on which we apply a myosin pulse to represent the cyclic medial myosin [15, 18, 24]. Such medial myosin pulls on cell–cell junctions and produce

cell area oscillation [24, 25]. Thus, our model accounts for both junctional and medial myosin, and in a way integrates the two hypotheses for cell edge contraction [8, 12, 15–17]. Note that we define the 'centroid' in a different sense than the geometric center of a polygon. It is initially at the center of the hexagon, but later moves according to the sum of spoke forces $\boldsymbol{f}_{mi}$.

2.1. Kinetic model

Based on observations of PCP development [6, 7, 9, 12–14], we include 4 species in our model: Shroom (S), Rok (R), myosin (m) and Baz (B), and define them on each of the cell edges. Actin is implicitly represented by the cell edges and spokes, and actin turnover is not modeled. Before intercalation starts, Shroom is known to act together with Rho to produce Rok polarity. We simplify this process by imposing the experimentally recorded polarized Shroom distribution [14] on the edges as an upstream trigger for Rok polarity. Thus, Rho-GTPases need not be explicitly accounted for. Furthermore, since the polarized Shroom distribution changes little during the intercalation process [14], we will keep a time-independent S distribution among the edges throughout the whole process, with a high, medium and low level assigned to the AP edges, shoulders and DV edges, respectively. This anisotropy is indicated graphically in figure 1(c). The other 3 species will evolve dynamically downstream of Shroom. In the stage of vertex resolution, the newly formed DV borders are known to accumulate E-cadherin and Baz, which promote and stabilize AJs on the DV edge. For simplicity, we do not explicitly account for the role of these AJs on DV edge elongation. Thus, E-cadherin need not be included in the model.

On each cell edge, we postulate the following kinetic equations that govern the dynamics of myosin, Rok, and Bazooka:

$$\frac{\mathrm{d}m}{\mathrm{d}t} = k_1 R - k_2 mB - k^- m, \tag{1}$$

$$\frac{\mathrm{d}R}{\mathrm{d}t} = q_r - k_r \mathrm{e}^{-S} R, \tag{2}$$

$$\frac{\mathrm{d}B}{\mathrm{d}t} = q_b - k_b RB. \tag{3}$$

In equation (1), the $k_1 R$ term represents the promotion of myosin by Rok, and $-k_2 mB$ reflects suppression of myosin by Baz [12]. The parameter k^- is the *load-dependent* dissociation rate of myosin [23, 26, 27]:

$$k^- = k_3 \mathrm{e}^{-k_4 f_{ij}}, \tag{4}$$

where f_{ij} is the tensile force on the edge between vertices i and j (see *Mechanical model* for details), and k_3 and k_4 are constants. The dependence of the myosin off-rate on the mechanical tension is a well-known fact [27, 28], and provides a positive feedback that promotes junctional myosin accumulation [8, 29]. Myosin localization onto the AP borders will increase the tension on it, which in turn enhances myosin accumulation.

In equation (2), q_r produces a steady source of Rok on the border, and the term $-k_r \mathrm{e}^{-S} R$ represents the polarizing effect of Shroom on Rok [14]. Through this inverse exponential term, Rok dissociation is suppressed where Shroom levels are high (on the AP border). The molecular pathway for Shroom activation of Rok is unclear at present, and there are no biological data to suggest a particular functional form. From a mathematical standpoint, an alternative form that directly promotes Rok by Shroom, such as $+k_r SR$, could work as well. However, the form of equation (2) is parsimonious; it balances the source term q_r to produce an equilibrium state without requiring additional terms. In equation (3), the constant q_b gives a steady source of Baz on the border and the term $-k_b RB$ quantifies the effect of Rok inhibiting Baz [12].

Taken together, these three equations encode the following effects documented in prior experiments:

- Polarity in Shroom produces polarity in Rok [14];
- Rok polarity in turn produces polarity in myosin [12];
- Rok inhibits Baz while Baz inhibits myosin [12].

As will be seen shortly, the inhibitions between Rok and Baz and between Baz and myosin will localize these proteins onto complementary edges and produce the desired PCP.

To reflect the periodic formation and dissolution of medial myosin [15, 16, 24], we define myosin on the spokes in the following form:

$$m_m = A_m \sin^2\left(\frac{t\pi}{T} + \varphi\right), \tag{5}$$

where the amplitude A_m, period T and phase φ will be chosen based on the experimental data of Fernandez-Gonzalez and Zallen [24]. Thus, the temporal variation of medial myosin is prescribed, and does not participate in the kinetics of the other species.

2.2. Mechanical model

As is typical of vertex models [22, 23], the cell deformation and rearrangement are realized through the movement of the vertices. Each vertex is subject to forces along the edges and spokes that meet at that vertex, as well as a pressure arising from the cytosol (figure 3). The force on an edge is the sum of a passive elastic force and an active tension due to junctional myosin:

$$f_{ij} = \mu\left(l_{ij} - l_0\right) + \beta\left(m_{ij} - m^e\right), \tag{6}$$

where μ is a constant elastic modulus, l_{ij} is the length of the edge, and l_0 is the rest length, uniform for all edges. β is the force per 'unit myosin', to be specified in the next subsection. A positive f_{ij} indicates tension whereas a negative value represents compression. As mentioned before, peripheral edges, i.e. those not shared by two neighboring cells in figure 1, have a force that is

half of the above because there is just one membrane and associated cortex. Equation (6) implies that a 'background' myosin level m^e exists without producing contraction force. Experiments by Blankenship *et al* [6] have shown a more or less uniform level of background myosin before cell intercalation begins (figure 1 E and E′ therein). The form of equation (6) explicitly manifests such a steady or equilibrium state. Algebraically, of course, having m^e is equivalent to modifying the resting length l_0 to account for the 'pre-strain' due to myosin contraction in equilibrium. In addition to the force f_{ij} on the edge, the medial myosin exerts a tension on the vertex toward the centroid: $f_m = \beta m_m$. Finally the pressure resists changes to the cell volume (or area in our 2D model): $p = \alpha (A_0 - A)$, where A_0 is the prescribed area of the cell, A is its current area, and the constant stiffness α is related to the cell's bulk modulus.

Each vertex undergoes inertialess motion determined by the driving forces described above and a viscous friction on the vertex:

$$\eta \frac{\mathrm{d}\boldsymbol{x_i}}{\mathrm{d}t} = \sum_j f_{ij} \frac{\boldsymbol{x_j} - \boldsymbol{x_i}}{\left|\boldsymbol{x_j} - \boldsymbol{x_i}\right|} + f_{mi}\boldsymbol{e}_{ci} + p\boldsymbol{e}_{ni}, \qquad (7)$$

where η is an effective viscosity, $\boldsymbol{e}_{ci}$ is the unit vector pointing from vertex i toward the centroid of the cell, and $\boldsymbol{e}_{ni}$ is an outward 'normal vector' that bisects the angle formed by the two edges meeting at vertex i (figure 3). The centroid moves according to an equation similar to equation (7), with the sum of myosin forces f_m on all the spokes on the right-hand side. Equations (4) and (6) reflect the positive feedback between the myosin level and mechanical force on cell borders. Myosin enrichment on AP borders, together with the medial myosin pulse (equation (5)), lead to their contraction.

Following the AP contraction, the neighbor swap is implemented as follows. Once the AP edge AA′ shrinks to a threshold length of $0.02l_0$, it is rotated by 90° to become a horizontal DV edge of length $0.02l_0$ (figures 1(b) and (c)). The new vertices A and A′ are then reconnected to nearby vertices C, C′ and B, B′ to form the shoulders. This circumvents the singularity of having a zero length for AA′ in the model. On the newly created DV edge, we put myosin, Rok and Baz to zero initially, and assign a low Shroom level according to the measured planar polarity [14].

The new DV edge elongates under two driving forces. First, the pulsating medial myosin in cell 4 and cell 2, anterior and posterior to the DV edge (figure 1(c)), pulls on the vertices A and A′ (see cartoon in figure 12(a)). Biologically, the medial myosin forces may disassemble the AJs on the shoulders and reassemble them on the DV edge. Second, the junctional myosin on the shoulders causes them to contract, thereby stretching the DV edge. The accumulation of myosin on the shoulders is dictated by the Shroom polarity at the start of cell intercalation [14]. As the DV edge grows, it develops a small but non-negligible myosin and a passive elasticity, both of which tend to resist the elongation of the edge.

Modeling the myosin and elastic forces on the nascent DV edge is subtle, and the two are somewhat related. Once the DV edge is fully grown, reaching length l_0, it should be treated the same way as all other edges, with the force given by equation (6). Prior to that, however, it is unclear what resting length to use for the passive elasticity. Biologically, the passive elasticity represents the AJs resisting elongation of the cell border. On the growing DV edge, new cell contact is being created by E-cadherin, and new AJs are being stabilized by Bazooka [2, 6, 7]. Thus, modeling the passive elasticity faithfully on the growing DV edge would involve the dynamics of AJ creation and maturation, and complicate the model considerably. Moreover, equation (6) expresses the myosin force using the 'excess myosin' above the equilibrium level m^e. As mentioned above, this amounts to the myosin prestress effectively reducing the resting length to a smaller value [30]. Thus, the myosin contraction force is implicitly related to the resting length, and equally difficult to model. To avoid these complexities, we have adopted the following scheme. The passive elastic force is assumed zero until the DV edge reaches the resting length, at which point the form $\mu(l_{ij} - l_0)$ comes into effect. Similarly the myosin contraction is neglected until m_{ij} reaches m^e on the DV edge, at which point the force $\beta(m_{ij} - m^e)$ is activated. This simple scheme ensures a continuous transition to the full formula of equation (6) on the growing DV edge.

In summary, our model follows the geometric setup of earlier vertex models [20–23]. Vertex motion and cell deformation are determined by driving forces due to junctional and medial myosin overcoming elastic resistance of the cell edges and viscous friction. What sets this model apart from most prior models is its integrating the polarization of chemical signals with the mechanics of cell deformation and movement. The polarization of proteins gives rise to the anisotropic contraction forces, and the forces and deformation modify the detachment rate of myosin in return, as indicated by the following diagram:

The dynamics is highly dissipative and open, with constant energy input into the system in the form of myosin contraction and chemical sources. This contrasts the conservative Hamiltonian dynamics that characterizes prior vertex models. Incorporating chemical and mechanical feedback reflects the biological reality more faithfully [31, 32], and follows the integrative approach advocated by Fletcher *et al* in a recent review [22].

Table 1. Value of parameters used in the model. See supplementary material for discussion of evaluating parameters from literature data.

Parameters		Values	Sources
Geometric parameters	l_0	4 μm	[6, 15, 24]
	A_0	41.6 μm^2	[24]
Mechanical parameters	η	4.63 nN s μm^{-1}	[20, 33]
	μ	0.031 nN μm^{-1}	
	β	0.324 nN	[20, 33–35]
	A_m	1	[8, 24]
	T	147 s	[24]
	φ	$\pi/4, 0, \pi/4, \pi/2$ for cell 1–4	[24]
	α	0.05 nN μm^{-2}	[36, 37]
Kinetic parameters	q_r	0.02 s^{-1}	
	q_b	0.02 s^{-1}	
	k_1	0.67 s^{-1}	[38]
	k_2	0.6 s^{-1}	
	k_3	0.27 s^{-1}	[26, 27]
	k_4	4.02 nN^{-1}	[26, 27]
	k_r	0.05 s^{-1}	
	k_b	0.05 s^{-1}	

2.3. Model parameters and numerics

The model parameters fall into three categories: geometric, mechanical and kinetic. Table 1 tabulates their 'baseline values', those used to produce most of the results to be presented. Where available, table 1 also lists the literature sources from which the baseline values are drawn. For some parameters, this process requires further explanation, which is given in the supplementary material available at stacks.iop.org/PB/12/056011/mmedia. In particular, the proteins are measured in a unit of 162 molecules; this corresponds to the number of myosin motors averaged over cell edges of various lengths.

Mathematically, the model consists of 97 ordinary differential equations for a total of 19 borders, 16 vertices and 4 centroids. The temporal evolution of the four-cell assembly is investigated by solving the differential equations using a second-order Runge–Kutta method. The time step has been varied to study temporal resolution, and $\Delta t = 0.01$ s is shown to be sufficiently fine. Since the T1 process takes tens of minutes in reality [2, 6], the simulation typically lasts for some 10^5 steps.

3. Results and analysis

The protocol of the simulation is as follows. Initially we impose a background Shroom level $S = 0.5$ on all edges, and let the system settle into a quasi-equilibrium, with a gentle oscillation due to the medial myosin pulse. This corresponds to the early Stage 6 observations of Blankenship *et al* [6] (figure 1 therein) before PCP initiates. At $t = 400$ s, we raise Shroom to $S = 1$ on the vertical edges, and 0.625 on the shoulders. Hence the PCP begins to develop. The AP edge AA′ contracts in time until its length falls below $0.02l_0$. This is taken to mark the formation of the vertex in the center of the four-cell assembly. The edge AA′ is then rotated by 90° into a new DV edge. The nascent DV edge initially bears zero myosin, Rok and Baz, and has the background $S = 0.5$ according to the experimentally observed Shroom polarity. As the DV edge proceeds to elongate, R, m and B develop subject to the low S level, resulting in a polarized distribution of the proteins among the edges of different orientation.

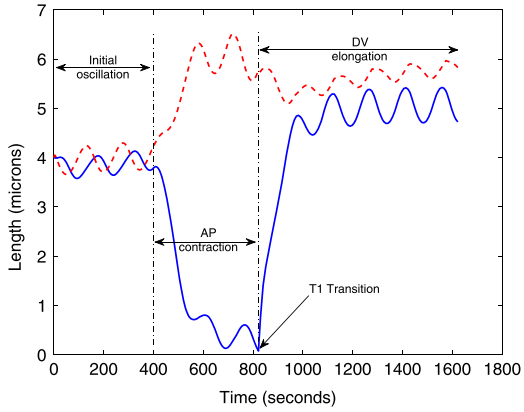

Figure 4. Temporal evolution of the length of the AP or DV edge (solid line) and the shoulder length (dashed line).

Figure 4 gives an overview of the entire simulation in terms of the evolving lengths of the AP (before T1 transition) or DV (after T1) edge and the shoulder. The evolution of the shape and size of the four-cell assembly is depicted in the supplementary movie SM. The dynamics exhibits three stages: initial oscillation, AP contraction and DV elongation, each to be discussed in turn.

3.1. Initial oscillation

The oscillation in figure 4, for $t < 400$ s, reflects the medial myosin pulse in each cell, and can be more clearly appreciated from supplementary movie SM1. This periodic forcing acts on an otherwise equilibrium state in which the myosin prestress and edge elasticity are in balance. It is worthwhile to specify this equilibrium quantitatively, as it pertains to the subsequent dynamics of myosin accumulation and AP contraction. Without the medial myosin pulse, an equilibrium state will prevail in which $S_{\rm eq} = 0.5$ on all the borders, and myosin, Baz and Rok are all at steady uniform levels. Besides, force balance at the vertices requires $f_{ij} = 0$ on all the edges. Setting the time derivatives to zero in equations (1)–(3) yields these equilibrium values:

$$R_{\rm eq} = \frac{q_r}{k_r} e^{S_{\rm eq}}, \tag{8}$$

$$B_{\rm eq} = \frac{q_b}{k_b R_{\rm eq}} = \frac{q_b}{q_r}\frac{k_r}{k_b} e^{-S_{\rm eq}}, \tag{9}$$

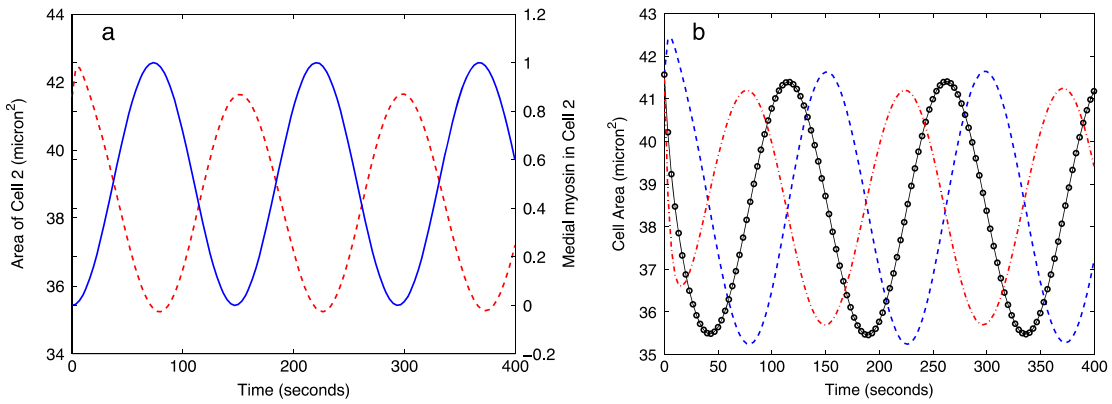

Figure 5. Initial oscillation prior to onset of planar cell polarity. (a) The cell area (dashed line) and medial myosin (solid line) in cell 2. (b) The areas of the four cells: cell 1 (solid line), cell 2 (dashed line), cell 3 (circles) and cell 4 (dash–dot line). The myosin pulses of cell 1 and 3 are in phase; they lead cell 2 by $\pi/2$ and trail cell 4 by $\pi/2$.

$$m_{\rm eq} = \frac{k_1 R_{\rm eq}}{k_2 B_{\rm eq} + k_3}. \tag{10}$$

In equation (10), the myosin off-rate $k^- = k_3$ under zero load (see equation (4)). From the kinetic parameters specified in table 1, we have $R_{\rm eq} = 0.659$, $B_{\rm eq} = 0.606$ and $m_{\rm eq} = 0.697$.

Imposing the medial myosin of equation (5) on this equilibrium state causes oscillations of the four-cell assembly. This is easily seen from the temporal variation of the cell areas in figure 5, where the medial myosin in cell 2 is also plotted for comparison. First, figure 5(a) shows that the cell area oscillates roughly anti-phase with the myosin pulse. This is illustrated for cell 2 but is true of all cells. The peak in myosin precedes the valley in cell area by some 6 s, a delay in cell contraction due to viscous friction and resistance of the neighbors. Second, based on experimental evidence [24, 29], we have designed the myosin pulse to be anti-phase between the two neighbors, cells 2 and 4 in figure 1. The areas of these two cells oscillate anti-phase as well; the slight offset is related to the contraction of cells 1 and 3, whose phase is midway between cells 2 and 4. The phase relationship is also clearly demonstrated in the animation of SM1. Finally, given the amplitude of medial myosin A_m and cell stiffness α used here, the cell area oscillates with an amplitude around 8.3%, in approximate agreement with the experimental data of Fernandez-Gonzalez and Zallen [24].

3.2. Polarization and AP contraction

At time $t = 400$ s, the Shroom level is raised from $S = 0.5$ to 1 on all vertical edges, and to 0.625 on the shoulders. The subsequent evolution of the chemical signals, depicted in figure 6, exhibits increasing anisotropy, with Rok and myosin up-regulated on the AP edges, and Baz down-regulated on them. The rise in myosin is thanks to both the accumulation of Rok and the tension-mediated positive feedback (equation (4)). On the shoulders, a similar trend is evident but the magnitude is smaller. The fluctuation of junctional myosin (figure 6(c)) is because the myosin detachment rate depends on the tension on the edges, which is in turn influenced by the medial myosin pulse. Note that the Rok development is mathematically decoupled from those of the other proteins, and can be solved analytically to yield an exponential form that grows asymptotically toward a steady level. The time scale for the development of Rok, Baz and myosin is determined by the rate constants, and is on the order of 5 min in figure 6, in rough agreement with observations [12]. Although there are no horizontal edges at this stage, the anisotropy represents the developing PCP in our simple four-cell assembly. After presenting results for DV elongation, we will return to the magnitude of the PCP by examining AP/DV ratios of the proteins.

Despite the positive feedback loop between myosin population and local tension [8], the AP-edge myosin does not grow without bound in a runaway instability, but rises gently toward a moderate level in figure 6(c). The supplementary material contains a brief analysis of the linear stability of the equilibrium state of equations (8)–(10). The dynamics of the system is dictated by the competition between the myosin-tension positive feedback and the inhibition of myosin by Bazooka. For the current T1 simulation, the parameter values ensure that the latter prohibits an instability and produces moderate myosin levels comparable with experimental measurements.

This does not imply that the runaway instability is necessarily absent in reality. In fact, rosettes require aligning a larger number of cells along a common edge, on which a stronger myosin contractile force develops [8]. It is quite possible, as surmised by Fernandez-Gonzalez *et al* [8], for such myosin accumulation to happen exponentially via the positive feedback described above. In reality, of course, exponential growth does not go unchecked, and attenuating factors will arise to cap the growth to a high but finite

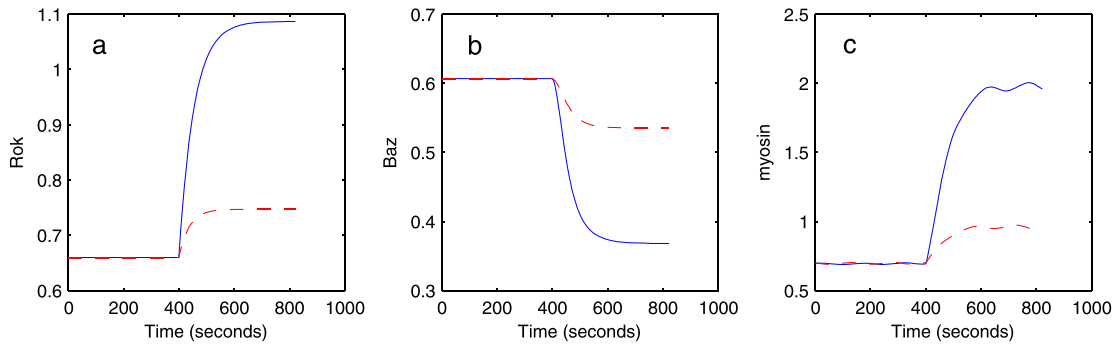

Figure 6. Development of (a) Rok, (b) Baz and (c) myosin on the AP edge AA′ (solid line) and the shoulder AB (dash line). The polarity in Shroom is imposed at $t = 400$ s.

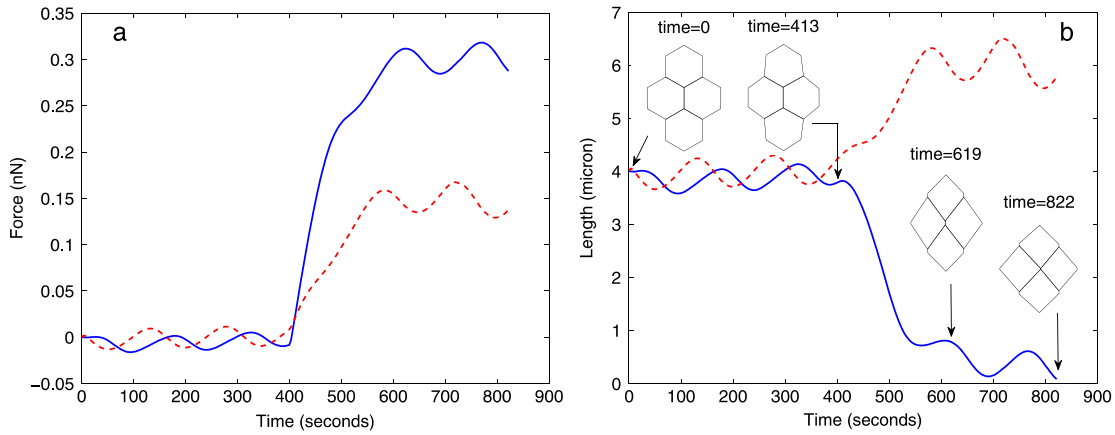

Figure 7. (a) Development of the forces on the AP edge (f_{AP}, solid line) and the shoulder (f_{SH}, dash line). (b) Variation of the AP length (l_{AP}, solid line) and the shoulder length (l_{SH}, dash line). Snapshots of the four-cell assembly are shown as insets.

level. For one, AP cell boundaries contract into vertices within finite time, inherently limiting the amount of myosin that they can accumulate.

Figure 7(a) shows the development of the forces f_{AP} on the AP edge AA′ and f_{SH} on the shoulder AB, each made of an active myosin force and a passive elastic force. Prior to the onset of Shroom anisotropy at $t = 400$ s, the forces are mostly negative (i.e. compressive) on both edges. This is because the undulating medial myosin pulls on the vertices and compresses the cell edges. Once the Shroom anisotropy is imposed, Rok and myosin grow on the AP edges (figures 6(a) and (c)), producing a steep increase in the contractile force f_{AP}. As a result, the AP edge contracts persistently till $t \approx 520$ s (figure 7(b)). This elicits stronger elastic resistance. So the rise in f_{AP} slows and eventually turns into an oscillation about a level mean. The oscillation is due to the medial myosin pulse, which causes not only the junctional myosin, but also the AP length l_{AP} to oscillate. The latter affects f_{AP} through passive elasticity. The AP contraction stage ends at $t \approx 822$ s, when l_{AP} reaches $0.02l_0$. In the process, the cell area contracts by roughly 10%. Movie SM2 illustrates the AP contraction graphically.

In the above process, the shoulder force f_{SH} mirrors f_{AP}, albeit smaller in magnitude. This is mostly because Shroom is lower on the shoulder than on the AP edge, and so are Rok and myosin. Interestingly, the shoulder length l_{SH} lengthens as l_{AP} contracts. Thanks to the geometric connectivity of the edges, the AP contraction pulls on the shoulders and elongates them. Experimentally, similar shoulder lengthening has been observed during rosette formation. The lengthening of the shoulder incurs an elastic tension, which helps increase the myosin population on the shoulder. This positive feedback has contributed to the rise of the shoulder force f_{SH}.

Certain aspects of the model prediction can be compared with experimental results. First, the AP contraction starts at $t = 400$ s and ends at $t = 822$ s. The duration of AP contraction, 422 s $\approx$ 7 min, agrees approximately with experimental measurements. For example, Blakenship *et al* [6] reported a range of 7.5 ± 0.3 min, and Bertet *et al* [2] gave 10 min. However, we should note that this agreement is partly the result of 'fitting' the parameter μ. In examining the mechanical parameters, we find the contraction rate to be very sensitive to the elastic modulus μ, but much less so to the viscosity η. This suggests that the

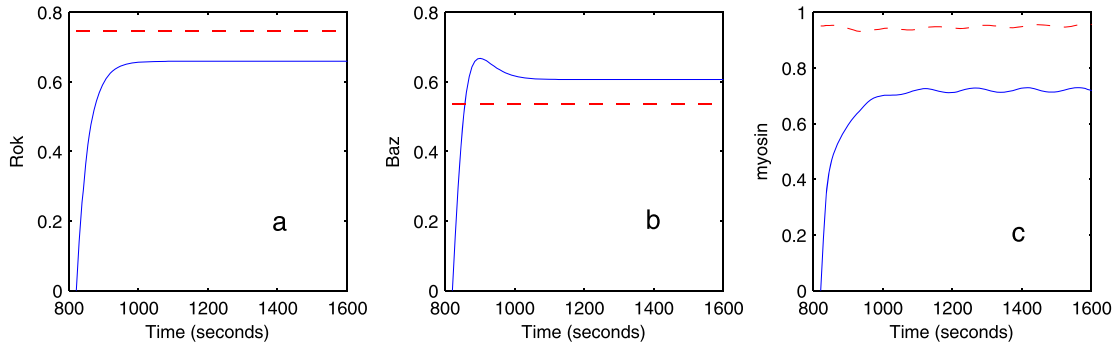

Figure 8. Evolution of (a) Rok, (b) Baz and (c) myosin on the nascent DV edge (solid line) and the shoulder (dash line) after the neighbor swap.

contraction is governed mostly by the balance between the myosin contraction and elastic resistance on the AP edge, and that the contribution of the viscous force may be relatively insignificant.

Second, the insets to figure 7(b) depict the evolving shapes of the cells and the four-cell 'tissue' during AP contraction. An animation can also be seen in movie SM2. In the model simulation, the 7 vertical edges, 1 in the center and 6 on the periphery, contract simultaneously. When the vertex forms at the center, the 4 cells have all assumed roughly diamond shapes, not the pentagon and heptagon anticipated in the cartoon of figure 1(c). As a whole, the four-cell assembly takes on a diamond shape as well. In reality, such shapes do occasionally appear at the moment of vertex formation; see figure 6 D′, E′ of Blankenship *et al* [6] (reproduced in figure 10 below) and figure 1(e) of Bertet *et al* [2]. However, typically the cell and tissue shapes are much less regular, since parallel vertical edges rarely contract simultaneously or at similar rates.

Third, we can estimate the AP/shoulder force ratio from figure 7(a). After an initial spike, the ratio settles into a regular oscillation between 1.7 and 2.3. Experimentally, Rauzi *et al* [20] measured the retraction velocity after laser ablation of the AP and shoulder edges, and estimated that the ratio between the average AP force and the average shoulder force is 2.26 (figure 6f′ therein), in close agreement with our model prediction. Disregarding the medial myosin forces, they argued that this ratio implies a force balance between the tension on the AP edge and the two shoulders. In our model, the medial myosin plays significant roles (more on this in section 3.4 below). Not surprisingly, the AP/shoulder force ratio is greater than the force-balance argument of Rauzi *et al* [20] would suggest.

3.3. DV elongation

After the neighbor swap, the newly created DV edge has initial values $m = R = B = 0$, as well as $S = 0.5$ according to the Shroom polarity [14]. Subsequently, m, R and B develop in time to quasi-steady levels given by equations (8)–(10) (figure 8). The rise of myosin, in particular, benefits from the positive feedback of equation (4). On the shoulders there are hardly any changes in the protein levels. The relatively high level of B and low levels of R and m on the DV edge are part of the PCP.

Table 2. Comparison of the planar cell polarity between model prediction and experiment.

Proteins	AP/DV ratio (model prediction)	AP/DV ratio (experimental data [14])
Rok	1.65	1.5–1.9
Bazooka	0.607	0.48–0.5
Myosin	2.74	1.6

The magnitude of the PCP can be quantified by the AP/DV ratio of various proteins. Comparing the quasi-steady m, R and B levels between figures 6 and 8, we list the AP/DV ratios in table 2. For the oscillating myosin, we use its mean value. The polarity in Rok matches the experimental range well, thanks to the Shroom polarity that is imposed. The Baz ratio is also fairly close to measured values. But the myosin ratio is over-predicted by some 70%. Part of this is because Simões *et al* [14] included edges oriented within 75°–90° of the AP axis in computing the average values for the 'vertical AP edges', and 0°–15° for the DV axis. The averaging has dulled the polarity somewhat. The experimental data show Baz to manifest the strongest anisotropy among the three proteins, with a DV/AP ratio of about 2. In our model, myosin turns out to have the strongest polarity. Given the simplicity of the kinetic model and the uncertainties in the kinetic parameters, perhaps the degree of quantitative agreement in the polarity is as much as we should expect.

Subject to this polarity, the tension and length of the DV edge and the shoulder evolve in time (figure 9). Note first the high and slowly rising tension f_{SH} on the shoulder, as well as the increasing shoulder length l_{SH}. Elongation of the shoulder is due to the area-preserving effect of the pressure p (see equation (7)). Cells 2 and 4, posterior and anterior to the DV edge, have essentially lost two edges in the T1 transition, changing from a hexagon to a quadrilateral. Thus, their edges lengthen to preserve their area, which oscillates

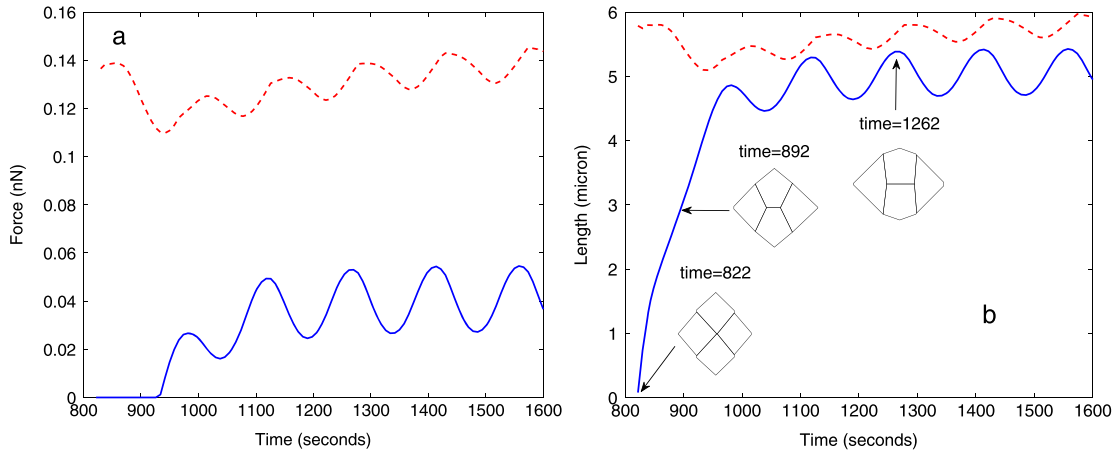

Figure 9. (a) Development of the forces on the nascent DV edge (f_{DV}, solid line) and the shoulder (f_{SH}, dashed line). (b) Variation of the DV length (l_{DV}, solid line) and the shoulder length (l_{SH}, dashed line). Snapshots of the four-cell assembly are shown as insets.

at about 10% below the initial area A_0. Elastic tension and junctional myosin contraction cooperate to produce f_{SH} on the shoulder, which drives the DV elongation. Another driving force comes from the medial myosin in cells 2 and 4, which pulls the vertices A′ and A apart. Medial myosin pulses are also responsible for the oscillations in figure 9. A detailed analysis of the roles of medial myosin will be given in the next subsection.

Under these forces, the DV edge extends at a rate that is determined by the viscous friction coefficient η, reaching the equilibrium edge length $l_0 = 4\,\mu$m at $t = 934$ s (figure 9(b)). Afterwards l_{DV} increases further, eventually fluctuating around a mean of about 5.07 μm. The initial rate of DV elongation, up to the first peak in l_{DV}, is roughly 0.03 μm s^{-1} in figure 9(b). This is about twice the experimentally measured value. The shoulder length l_{SH} increases slowly in time while oscillating, reaching a mean of 5.78 μm at the end of the simulation. Thus, both the DV and the shoulder edges are under elastic tension. The process of DV elongation is also shown graphically in Movie SM3.

To estimate the duration of DV elongation, we note that it starts at $t = 822$ s, reaches its first peak ($l_{DV} = 4.86\,\mu$m) at 982 s, a higher second peak ($l_{DV} = 5.29\,\mu$m) at 1118 s, and a still higher third peak ($l_{DV} = 5.38\,\mu$m) at 1262 s. Afterwards the peaks change little and the oscillation becomes nearly periodic around of a mean of about 5.07 μm. If we take the third peak as the end of the elongation stage, it has taken 440 s. This is in rough agreement with experimental observations: 6–7 min in Blankenship *et al* [6] (figure 6 D′, D″, E′, E″), and around 10 min in Bertet *et al* [2] (figures 1(e), (f)). While we have tuned the elastic modulus μ to produce the correct duration of AP contraction, no such tuning is done for the DV elongation stage.

Further comparisons with experiments can be made about the anisotropy in contractile forces in the four-cell assembly. From the quasi-steady myosin levels on the AP edge (figure 6(c)) and DV edge (figure 8(c)), the peak myosin contractile force is 0.638 nN on the AP edge and 0.233 nN on the DV edge. These are almost twice the measured forces of Bambardekar *et al* [33]: 324 pN on AP edges and 127 pN on DV edges. The discrepancy is mainly because the experimental data are averages over edge orientations up to 45° from the AP and DV axes, and probably also over edges of different lengths and thus different degrees of contraction or elongation [33]. In contrast, our values are the peak forces on the shortest AP and longest DV edges. Rauzi *et al* [20] measured the recoil velocity upon nano-dissection for a range of edge length. The difference between the peak and average velocities is easily over a factor of 2. Besides, the error bars on the data in [33] suggest peak AP and DV forces of roughly 420 and 250 pN, respectively, which are closer to the model predictions. The AP/DV force ratio is about 2.74 in our model prediction. Experimentally, Bambardekar *et al*'s ratio is 2.55 [33], while Fernandez-Gonzalez *et al* [8] measured an AP/DV force ratio of 1.7. Thus, the model over-predicts the AP/DV force ratio somewhat. This is consistent with over-predicting the AP/DV ratio for myosin in table 2.

We can also examine the magnitude of convergent-extension. Overall the germband elongates along the AP axis and narrows along the DV axis [1]. For our four-cell tissue, we define its aspect ratio as the end-to-end vertical dimension divided by the horizontal dimension. The change in aspect ratio can then be compared with experiments (figure 10). The model predicts an aspect ratio of 1.44 at the start, 1.12 at the point of central vertex formation, and 0.79 at the end. The overall change in tissue shape can be quantified by defining a *convergent-extension ratio* r_{CE} as the aspect ratio at the start divided by that at the end. Then our model predicts $r_{CE} = 1.82$. Experimentally, the top row of figure 10(b) show the aspect ratios as 1.94 (frame D), 1.50 (D′) and 1.12 (D″), with $r_{CE} = 1.73$.

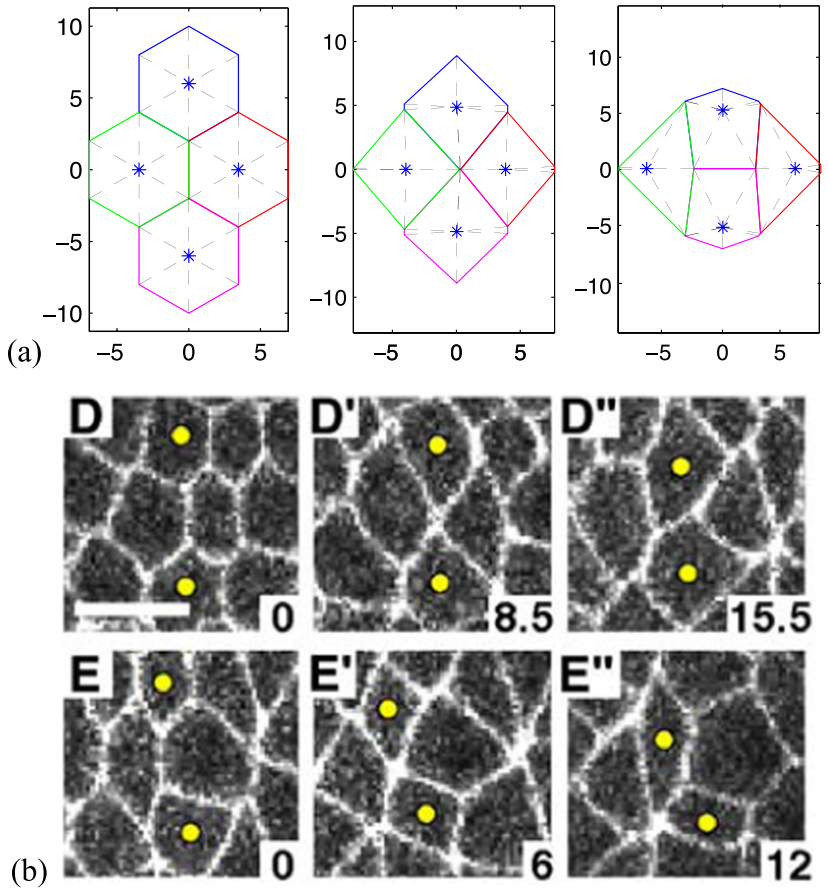

Figure 10. Comparison of the tissue shape during T1 transition. (a) Model prediction of the shape of the four-cell assembly at the start of AP contraction ($t = 0$), central vertex formation (7.0 min) and the end of DV extension (14.4 min). The coordinates are in μm. (b) Two series of experimental snapshots showing T1 transition, adapted from figure 6 of Blankenship *et al* [6] with permission, © Elsevier Inc. The circles mark two cells that correspond to our cell 1 and 3 in figure 1. The scale bar is 10 μm, and the numbers in each frame indicate time in minutes since the start of the T1 process.

For the bottom row, the aspect ratios are 1.55 (E), 1.0 (E′) and 0.92 (E″), with $r_{CE} = 1.68$. Similar images from Bertet *et al* [2] (figures 1(d)–(f)) give the three aspect ratios as 1.46, 1.28 and 1.0, with $r_{CE} = 1.46$, and Zallen and Blakenship [7] reported an average of $r_{CE} = 1.56$. The experimental data show considerable scatter. But nevertheless, the model appears to over-predict systematically the total amount of convergent-extension r_{CE}. This seems consistent with the over-prediction of the myosin polarity (table 2) and the anisotropy in contractile forces. Besides, our four-cell assembly is isolated from surrounding tissues, and this artificial setup may have contributed to the large r_{CE}. In our model, the peripheral vertical edges contract simultaneously with the central AP edge. In reality, AP contraction is not synchronized among neighbors. Thus, the lack of convergent-extension in the surrounding cells will hinder the intercalating cells and depress their r_{CE}.

3.4. Junctional myosin versus medial myosin

In the Introduction, we have motivated the present study by the following questions:

- How does PCP lead to anisotropic forces on the cells?
- How do these forces cause T1 transition, i.e., AP contraction and DV elongation?
- Can T1 transition be predicted quantitatively using reasonable parameter values?
- What are the roles of junctional and medial myosin in the T1 process?

The first three questions have been answered in the preceding subsections, and now we turn to the last.

Let us start by analyzing the various forces that govern AP contraction. For brevity, we will focus on the forces acting on vertex A of figure 1(a) (see schematic in figure 11(a)), keeping in mind that a similar set of forces are at work on vertex A′. These include the AP edge force f_{AP}, the shoulder force f_{SH} on the edges AB and AC, and the medial myosin force on the three spokes that end in A. $f_{AP} = f_{my} + f_{el}$ is made of the junctional myosin force $f_{my} = \beta(m - m^e)$ and the elastic force $f_{el} = \mu(l - l_0)$ on AA′. It turns out that AP contraction is driven by the junctional myosin force f_{my} overcoming several opposing forces: f_{el} on the AP

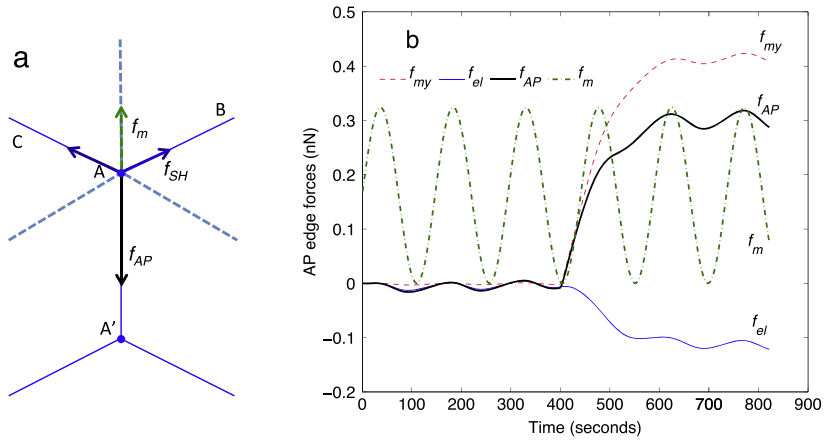

Figure 11. Force analysis of AP contraction. (a) Schematic showing the forces acting on node A. The three dashed lines indicate spokes, and only the medial myosin force on the vertical spoke is shown by an arrow. (b) Evolution of the junctional myosin force f_{my}, elastic force f_{el} and their sum f_{AP} on the AP edge AA′. The medial myosin force f_m in cell 1 is also shown.

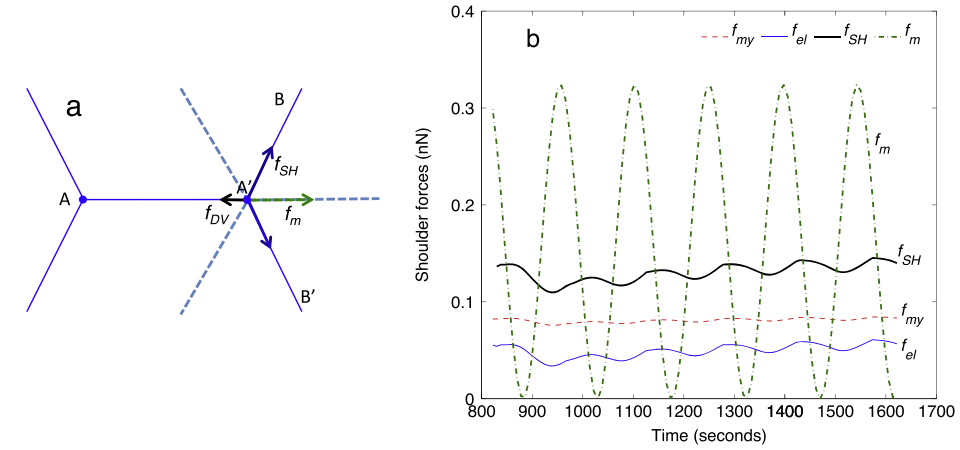

Figure 12. Force analysis of DV elongation. (a) Schematic showing the forces acting on node A′. The three dashed lines indicate spokes, and only the medial myosin force on the horizontal spoke is shown by an arrow. (b) Evolution of the junctional myosin force f_{my}, elastic force f_{el} and their sum f_{SH} on the shoulder A′B. The medial myosin force f_m in cell 2 is also shown.

edge, the medial myosin force f_m in cell 1, and the shoulder force f_{SH} on edges AB and AC. Figure 11(b) shows that f_{my} dominates f_{el} in magnitude, and is also more than twice the mean value of the medial myosin force f_m. The shoulder force f_{SH}, not shown in the plot, is only about half the magnitude of f_{my}. The spokes to the left and right of the AP edge initially contribute a small force assisting AP contraction, but this effect declines as the AP edge shrinks and these two spokes become nearly horizontal. The dominance of the AP junctional myosin bespeaks the positive feedback between myosin and the tension that it generates [8].

Although the medial myosin force f_m is much smaller than the junctional myosin force f_{my}, its role is nevertheless significant. As the AP edge contracts, the driving force is increasingly matched by the resisting forces. Thus, even a relatively small resistance from the medial myosin makes a great difference. This has been verified by changing the intensity of the medial myosin pulse of equation (5). Raising A_m from the baseline value of 1 to 1.2 slows down AP contraction so that it lasts 575 s (compared with 422 s for $A_m = 1$). Conversely, $A_m = 0.8$ hastens the AP contraction to within 280 s. Removing medial myosin altogether results in an AP contraction of only 192 s. Therefore, while the junctional myosin drives AP contraction, the medial myosin contributes a resistance that is especially significant at the end.

A similar force analysis can be done for DV elongation by focusing on the end node A′ of the DV edge AA′ (see schematics in figures 1(c) and 12(a)). DV lengthening is driven by the shoulder tension f_{SH} and the medial myosin force f_m in cell 2, against resistance due to DV edge tension f_{DV} and medial myosin forces from cells 1 and 3. The driving forces are shown in figure 12(b), with f_{SH} and f_m making similar contributions (∼0.15 nN). The DV tension f_{DV} is much smaller in magnitude (∼0.04 nN), and thus the resistance comes mainly from the medial myosin in cells 1 and 3, above and below the DV edge. As the DV edge lengthens, the orientation of the forces evolves such that f_{SH} becomes less efficient at elongating the DV edge, while

the medial myosin in cells 1 and 3 grows more potent in resisting it. The force balance produces a DV length that fluctuates around 5.07 μm, shown in figure 9(b). To summarize, in DV elongation, medial myosin plays a more important role than junctional myosin. Medial myosin from cells anterior and posterior to the DV edge acts to lengthen it, while that from the cells dorsal and ventral to it resists the lengthening. The junctional myosin on the shoulders helps with the elongation at the start, but its effect dies down later. The myosin on the DV edge itself is small in magnitude and plays a negligible role.

It is interesting to speculate on the biology behind the competing roles of medial myosin from different neighbors. Medial myosin in the cells anterior and posterior to the DV edge may help disassemble AJs along the shoulders, and then facilitate the forming of new AJs along the growing DV edge as the cell membranes fuse between cell 1 and 3. Similar scenarios have been documented for the assembly of new junctions between daughter cells after cell division [39] and in cell–cell adhesion [19]. Meanwhile, medial myosin in the cells above and below the DV edge may pull on the new AJs and hinder their growth. Increasing the medial myosin amplitude A_m increases the speed of DV elongation as well as the average l_{DV} in the end. Removing the medial myosin altogether slows down DV elongation considerably, with l_{DV} approaching steady state only after some 1000 s. Thus, the pulling medial myosin from cells 2 and 4 has an upper hand over the resisting medial myosin from cells 1 and 3. In reality, this predominance may be even stronger than predicted here, as the medial myosin pulse is anisotropic with stronger contraction along the AP axis than the DV axis [15, 24]. This feature is not included in the current model.

4. Conclusion

In this paper we present a mathematical model for the T1 process in cell intercalation during *Drosophila* GBE. It involves simple chemical kinetics for several protein species: Shroom, Rho-kinase, Bazooka and myosin-II, as well as the mechanics of cell deformation and movement. The overall goal is to predict key features of experimental observations using a minimal set of assumptions. More specifically, we have investigated several fundamental questions on the PCP, its role in generating anisotropic forces in the tissue, and the subsequent neighbor-swapping intercalation. These are answered, partially at least, by the main results of the study, which can be summarized as follows:

(a) The model provides a coherent framework for understanding cell intercalation, which comprises three key components: (i) an anisotropic Shroom distribution leads to spontaneous development of PCP; (ii) this in turn produces an anisotropy in myosin contractile forces on the cell borders, assisted by a positive feedback on myosin through a tension-dependent detachment rate; (iii) the anisotropic forces drive cell deformation, movement and intercalation, producing convergent extension. Each component is elucidated on the basis of biochemical and mechanical principles.

(b) The model predictions agree well with experimental observations. The degree of AP/DV polarity, the durations of AP contraction and DV elongation, and the magnitude of convergent extension are captured with quantitative accuracy.

(c) By analyzing the roles of two distinct pools of myosin—the junctional and the medial—the model suggests that the former drives contraction of the AP edges, but the latter is important to DV edge elongation.

By including the biochemical development of polarization, the current model has an advantage over purely mechanical models that are typically concerned only with how an elastic network deforms and relaxes under prescribed contractile forces [20]. Now the tension anisotropy, a key input parameter in mechanical models, can be predicted from the polarization of the signal proteins. The predicted chemical polarity and tension anisotropy can be compared with experimental data, and good agreement is found in both cases. An additional novelty of the current model is the inclusion of medial myosin. This allows its role to be examined relative to that of the junctional myosin, thus addressing one of the outstanding questions in the literature.

Of necessity, the model contains several assumptions. Foremost among them is the use of a minimalist four-cell 'tissue', which leaves out longer-range cell interactions. In particular, we have consciously left out the dynamics of rosette formation and resolution [6, 7]. A logical extension is to model a more realistic tissue of many cells such that boundary conditions imposed at the tissue edge do not seriously affect cell intercalation in the interior. In such a setup, one may probe the mechanisms for rosette formation and resolution, using a prior mechanical model as guideline [40]. The spatial heterogeneity and temporal stochasticity among the cells can be introduced through phase differences in the medial myosin pulse that conform statistically to measured anti-phase correlations, as well as random delays in the onset of polarization and AP contraction. Moreover, simulating a large number of T1 and rosette processes may allow us to predict the overall extension of the germband as a whole, as has been done using a purely mechanical model [20].

One can identify at least three additional shortcomings of the model. (i) It does not seek to elucidate the origin of PCP beyond an anisotropic localization of Shroom [14]. This begs the question of whence the

Shroom polarity comes. Recent evidence points to the Toll receptors as essential for PCP [41], although their downstream target is unclear. (ii) The model ignores the localization of E-cadherin on the DV edge and the stabilization of new AJs, which may be important in reality [2]. (iii) The model has minimal account of spatial gradients, only through phase differences in the medial myosin pulse among neighboring cells. Recent work has suggested roles for medial myosin flows in cell intercalation [15, 16, 18]. This is not explored in the model.

Shortcomings (i) and (ii) are difficult to address, as they reflect current lacunas in our biological knowledge. Thus, the modeling exercise of this paper has suggested future experiments to explore several outstanding questions. For example, what initiates the polarity of upstream signals? How do new AJs form and stabilize as the DV edge grows? How does the pulling force due to medial myosin affect this process? What is the state of forces on the DV edge due to myosin contraction and elasticity? The answers to the latter questions will provide a biological mechanism for DV elongation that is currently missing. Shortcoming (iii) can be remedied by allowing spatial variations inside each cell. This calls for a higher-resolution description based on partial differential equations, with greater mathematical complexity and computational cost. But it will afford the opportunity to explore the origin and consequences of the myosin flow. Interesting questions include how interaction between medial myosin and the cell periphery drives the myosin flow, and how medial myosin merges with junctional myosin [15, 18].

Acknowledgment

This study was supported by NSERC, the Canada Research Chair program, and the Canada Foundation for Innovation. We thank Thomas Lecuit, Len Pismen and Jessica Yu for discussions, and an anonymous referee for suggesting the wiring diagram on p 5. JJF acknowledges additional support by the Peter Wall Institute for Advanced Studies during his tenure as Wall Scholar.

References

[1] Irvine K D and Wieschaus E 1994 Cell intercalation during Drosophila germband extension and its regulation by pair-rule segmentation genes *Development* **120** 827–41
[2] Bertet C, Sulak L and Lecuit T 2004 Myosin-dependent junction remodelling controls planar cell intercalation and axis elongation *Nature* **429** 667–71
[3] Butler L C, Blanchard G B, Kabla A J, Lawrence N J, Welchman D P, Mahadevan L, Adams R J and Sanson B 2009 Cell shape changes indicate a role for extrinsic tensile forces in *Drosophila* germ-band extension *Nat. Cell Biol.* **11** 859–64
[4] da Silva S M and Vincent J P 2007 Oriented cell divisions in the extending germband of *Drosophila Development* **134** 3049–54
[5] Dennin M 2004 Statistics of bubble rearrangements in a slowly sheared two-dimensional foam *Phys. Rev.* E **70** 041406
[6] Blankenship J T, Backovic S T, Sanny J S, Weitz O and Zallen J A 2006 Multicellular rosette formation links planar cell polarity to tissue morphogenesis *Dev. Cell* **11** 459–70
[7] Zallen J A and Blankenship J T 2008 Multicellular dynamics during epithelial elongation *Semin. Cell Dev. Biol.* **19** 263–70
[8] Fernandez-Gonzalez R, Simões S de M, Röper J-C, Eaton S and Zallen J A 2009 Myosin II dynamics are regulated by tension in intercalating cells *Dev. Cell* **17** 736–943
[9] Vichas A and Zallen J A 2011 Translating cell polarity into tissue elongation *Semin. Cell Dev. Biol.* **22** 858–64
[10] Shannon E W and Hardin J 2014 Cell intercalation from top to bottom *Nat. Rev. Mol. Cell Biol.* **15** 34–48
[11] Wallingford J B 2012 Planar cell polarity and the developmental control of cell behavior in vertebrate embryos *Ann. Rev. Cell Dev. Biol.* **28** 627–53
[12] Simões S de M, Blankenship J T, Weitz O, Farrell D L, Tamada M, Fernandez-Gonzalez R and Zallen J A 2010 Rho-kinase directs Bazooka/Par-3 planar polarity during *Drosophila* axis elongation *Dev. Cell* **19** 377–88
[13] Zallen J A and Wieschaus E 2004 Patterned gene expression directs bipolar planar polarity in *Drosophila Dev. Cell* **6** 343–55
[14] Simões S de M, Mainieri A and Zallen J A 2014 Rho GTPase and Shroom direct planar polarized actomyosin contractility during convergent extension *J. Cell Biol.* **204** 575–89
[15] Rauzi M, Lenne P-L and Lecuit T 2010 Planar polarized actomyosin contractile flows control epithelial junction remodelling *Nature* **468** 1110–5
[16] Levayer R and Lecuit T 2012 Biomechanical regulation of contractility: spatial control and dynamics *Trends Cell Biol.* **22** 61–81
[17] Guillot C and Lecuit T 2013 Mechanics of epithelial tissue homeostasis and morphorgenesis *Science* **340** 1185–9
[18] Levayer R and Lecuit T 2013 Oscillation and polarity of E-cadherin asymmetries control actomyosin flow patterns during morphogenesis *Dev. Cell* **26** 162–75
[19] Baum B and Georgiou M 2011 Dynamics of adherens junctions in epithelial establishment, maintenance, and remodeling *J. Cell Biol.* **192** 907–17
[20] Rauzi M, Verant P, Lecuit T and Lenne P-F 2008 Nature and anisotropy of cortical forces orienting *Drosophila* tissue morphogenesis *Nat. Cell Biol.* **10** 1401–10
[21] Solon J, Kaya-Copur A, Colombelli J and Brunner D 2009 Pulsed forces timed by a ratchet-like mechanism drive directed tissue movement during dorsal closure *Cell* **137** 1331–42
[22] Fletcher A G, Osterfield M, Baker R E and Shvartsman S Y 2014 Vertex models of epithelial morphogenesis *Biophys. J.* **106** 2291–304
[23] Wang Q, Feng J J and Pismen L M 2012 A cell-level biomechanical model of *Drosophila* dorsal closure *Biophys. J.* **103** 2265–74
[24] Fernandez-Gonzalez R and Zallen J A 2011 Oscillatory behaviors and hierarchical assembly of contractile structures in intercalating cells *Phys. Biol.* **8** 045005
[25] Sawyer J K, Choi W, Jung K-C, He L, Harris N J and Peifer M 2011 A contractile actomyosin network linked to adherens junctions by Canoe/afadin helps drive convergent extension *Mol. Biol. Cell* **22** 2491–508
[26] Veigel C, Molloy J E, Schmitz S and Kendrick-Jones J 2003 Load-dependent kinetics of force production by smooth muscle myosin measured with optical tweezers *Nat. Cell Biol.* **5** 980–6
[27] Kovacs M, Thirumurugan K, Knight P J and Sellers J R 2007 Load-dependent mechanism of nonmuscle myosin 2 *Proc. Natl Acad. Sci. USA* **104** 9994–9
[28] He L, Wang X, Tang H and Montell D 2010 Tissue elongation requires oscillating contractions of a basal actomyosin network *Nat. Cell Biol.* **12** 1133–42
[29] Kasza K E and Zallen J A 2011 Dynamics and regulation of contractile actin-myosin networks in morphogenesis *Curr. Opin. Cell Biol.* **23** 30–8
[30] Morozov K I and Pismen L M 2011 Cytoskeleton fluidization versus resolidification: prestress effect *Phys. Rev.* E **83** 051920

[31] Salbreux G, Barthel L K, Raymond P A and Lubensky D K 2012 Coupling mechanical deformations and planar cell polarity to create regular patterns in the zebrafish retina *PLoS Comput. Biol.* **8** e1002618
[32] Aegerter-Wilmsen T, Heimlicher M B, Smith A C, de Reuille P B, Smith R S, Aegerter C M and Basler K 2012 Integrating force-sensing and signaling pathways in a model for the regulation of wing imaginal disc size *Development* **139** 3221–31
[33] Bambardekar K, Clément R, Blanc O, Chardès C and Lenne P-F 2015 Direct laser manipulation reveals the mechanics of cell contacts *in vivo Proc. Natl Acad. Sci. USA* **112** 1416–21
[34] Uyeda T Q, Kron S J and Spudich J A 2990 Myosin step size. Estimation from slow sliding movement of actin over low densities of heavy meromyosin *J. Mol. Biol.* **214** 699–710
[35] Vinzenz M *et al* 2012 Actin branching in the initiation and maintenance of lamellipodia *J. Cell Sci.* **125** 2775–85
[36] Girard P P, Cavalcanti-Adam E A, Kemkemer R and Spatz J P 2007 Cellular chemomechanics at interfaces: sensing, integration and response *Soft Matter* **3** 307–26
[37] Bittig T, Wartlick O, Kicheva A, González-Gaitán M and Jülicher F 2008 Dynamics of anisotropic tissue growth *New J. Phys.* **10** 063001
[38] Amano M, Ito M, Kimura K, Fukata Y, Chihara K, Nakano T, Matsuura Y and Kaibuchi K 1996 Phosphorylation and activation of myosin by Rho-associated kinase (Rho-kinase) *J. Biol. Chem.* **271** 20246–9
[39] Herszterg S, Leibfried A, Bosveld F, Martin C and Bellaiche Y 2013 Interplay between the dividing cell and its neighbors regulates adherens junction formation during cytokinesis in epithelial tissue *Dev. Cell* **24** 256–70
[40] Trichas G *et al* 2012 Multi-cellular rosettes in the mouse visceral endoderm facilitate the ordered migration of anterior visceral endoderm cells *PLoS Biol.* **10** e1001256
[41] Paré A C, Vichas A, Fincher C T, Mirman Z, Farrell D L, Mainieri A and Zallen J A 2014 A positional Toll receptor code directs convergent extension in *Drosophila Nature* **515** 523–7

Supplementary materials for

A Biomechanical Model for Cell Polarization and Intercalation during *Drosophila* Germband Extension

Haihan Lan[1], Qiming Wang[2] , Rodrigo Fernandez-Gonzalez[3,4] and James J. Feng[5,6]

1) Department of Electrical and Computer Engineering, University of British Columbia, Vancouver, BC V6T 1Z2, Canada

2) Department of Mathematics and Statistics, York University, Toronto, ON M3J 1P3, Canada

3) Institute of Biomaterials & Biomedical Engineering, University of Toronto, Toronto, ON M5S 3G9, Canada

4) Department of Cell & Systems Biology, University of Toronto, Toronto, ON M5S 3G5, Canada

5) Department of Mathematics, University of British Columbia, Vancouver, BC V6T 1Z2, Canada

6) Department of Chemical and Biological Engineering, University of British Columbia, Vancouver, BC V6T 1Z3, Canada

A. Evaluation of model parameters

To the greatest extent possible, we have based the model parameters of Table 1 on experimental literature. The following explains their evaluation.

Among the mechanical parameters, the period T and phase difference φ among neighboring cells are taken from Ref. [24]. The amplitude of medial myosin pulse A_{m} is chosen to be on the same order of magnitude as the junctional myosin [8,24]. The parameter α represents the stiffness of the cell, and is thus estimated based on its bulk modulus [36,37]. The estimation of β and η is related. Bambardekar et al. [33] reported tension on AP edges during cell intercalation, f_{AP} = 0.324 nN. As such tension is expected to vary with edge length, with shorter, more contracted edges being under greater tension [20], the reported f_{AP} is taken to be an average over the range of edge lengths. We define the amount of myosin producing such an average tension to be 1 unit. This naturally determines the value of β = 0.324 nN per unit. Furthermore, from the average recoil speed after laser ablation [20], v_{av} = 0.07 μm/s, we estimate the viscosity $\eta = f_{AP}/v_{av}$.

The number of myosin molecules contained in such a unit can be estimated in two independent ways. First, each myosin motor generates about 2 pN of force [26,27]. Thus the average f_{AP} = 0.324 nN implies 162 myosin motors in the unit. Second, Uyeda *et al*. [34] estimated the density of myosin on actin filaments. Their results fall in a wide range, with 40 motors per μm being a reasonable medium. Vinzenz *et al.* [35] showed that the typical actin bundle encircling wounds in melanoma and fibroblast cells consists of about 10 actin filaments of length ~ 1 μm. This length is consistent with our geometric setup. So we expect about 400 myosin motors in a unit, on the same order of magnitude as the first estimation. Hence, we take 162 molecules as the unit for myosin, as well as Shroom, Rok and Bazooka in the kinetic equations. For brevity, this unit has been omitted when discussing the protein levels in the text.

The elastic modulus μ is difficult to evaluate because its physical origin cannot be clearly delineated from cell components. Note that this is the elastic modulus of the cell edge, not the overall cell modulus commonly measured by deforming the whole cell [36]. Despite its obscure biological basis, cell edge elasticity is widely used in vertex models, as "line tension" or "cortical

tension", possibly thanks to the convenience that it offers in defining an equilibrium shape and area to the cell [20,21], which in reality may depend on surrounding cells and longer-range geometric and mechanical constraints. Thus, we have used μ as the only adjustable parameter among the mechanical parameters. Its value is chosen such that the duration of AP contraction matches experimental data. Implicitly, it represents additional resistance to cell contraction and movement due to surrounding tissues that are absent from our model.

Of the kinetic parameters, only k_1, k_3 and k_4 can be evaluated from experimental data. In particular, k_4 represents the sensitivity of the myosin detachment rate to the tensile force of a cell edge. It is derived from the measured force-sensitivity for a single myosin motor [27]. The source terms q_r and q_b and rate constants k_2, k_r and k_b have been chosen to produce reasonable time scales for PCP development and the degree of polarity.

B. Stability of the equilibrium state

As noted in the main text, we can define a steady equilibrium state by ignoring the medial myosin pulse for the time being, and imposing $S_{eq} = 0.5$ on all the borders. This state is characterized by the Rok, Baz and myosin levels given in Eqs. (8–10).

Now we can examine the stability of the equilibrium state, as this sheds light on the nature of the polarization that follows the imposition of Shroom anisotropy. As tension in the actin filament suppresses myosin detachment (Eq. 4), Fernandez-Gonzalez *et al.* [8] suggested a positive feedback mechanism to explain the accumulation of myosin on AP edges. A small addition to the myosin population would elevate the tension, which in turn encourages more myosin to stay attached, raising the tension even further. This could lead to a runaway instability in the equilibrium state. Such a scenario is possible in our mathematical model, but did not happen for the parameter values chosen here.

To see this, we linearize Eqs. (1–3) at the equilibrium, and compute the Jacobian matrix of the system of ordinary differential equations:

$$\mathbf{J} = \begin{bmatrix} k_3 k_4 \beta m_{eq} - k_3 - k_2 B_{eq} & k_1 & -k_2 m_{eq} \\ 0 & -k_r e^{-S_{eq}} & 0 \\ 0 & -k_b B_{eq} & -k_b R_{eq} \end{bmatrix},$$

whose eigenvalues are simply the three diagonal elements. For the parameters in Table 1, these are all negative: $\boldsymbol{\lambda} = (-0.389, -0.0606, -0.0659)$. Thus the system is linearly stable near the equilibrium state. Mathematically, the positive feedback is coded in the last term of Eq. (1), and reflected by the first term in the diagonal element $\lambda_1 = k_3 k_4 \beta m_{eq} - k_3 - k_2 B_{eq}$ of the Jacobian. For a larger β or a larger k_4, corresponding respectively to stronger myosin contraction or heightened force-sensitivity of myosin detachment, the first term can become large enough to overcome Bazooka's effect in suppressing myosin (the $-k_2 B_{eq}$ term). Then λ_1 may turn positive, and the system will become unstable, with exponential growth of myosin on AP edges. We choose our parameters to stay in the stable regime so as to predict an AP/DV polarity that is comparable with the typically modest anisotropy measured in PCP (cf. Table 2 in subsection III.C of the main text). For example, the measured AP/DV myosin ratio is only 1.5 – 1.6 [14,15]. Therefore, a runaway instability in our model would appear unrealistic. Instead, we have opted for the milder form of anisotropy, which develops in reaction to the imposed Shroom polarity.

C. Interaction with surrounding tissue

A drastic simplification of the model is the omission of other cells surrounding the four-cell assembly, essentially isolating the latter. In reality, the surrounding cells interact with those in the assembly in the same way as those inside the assembly interact among themselves. As an attempt to capture some of the effects of the surrounding tissue, we put the four-cell assembly at the center of a rigid circle, and deployed a set of elastic springs that connect each outer node to the outer boundary, in the spirit of the amnioserosa model of Solon et al. [21]. An example is shown below in Fig. S1, with the external springs initially oriented toward the center of the circle. They have the same elastic modulus μ as the internal edges, and are relaxed when the four-cell assembly is undeformed at the start.

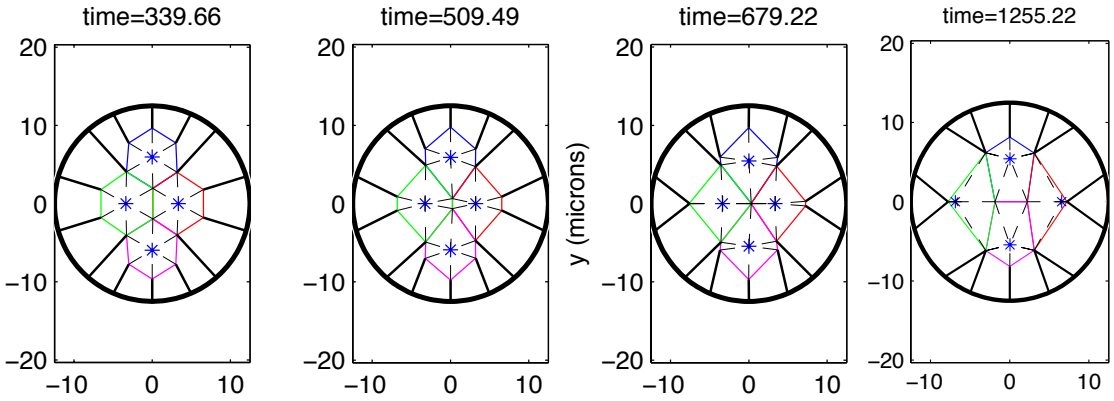

Figure S1. An attempt to represent the surrounding tissue using elastic springs. The radius of the outer boundary is $3.125l_0$. All other parameters and conditions of this simulation are the same as in Fig. 4 of the main text.

The external springs turn out to have only a modest effect; they mostly reduce the anisotropy of the deformation. At the point of the T1 transition (time=679.22 s), the four-cell assembly has contracted less along the vertical axis, down from 10.6% contraction without springs to 3.5% contraction with spring. The DV edge eventually attains a shorter length slightly below l_0=4 μm, compared with 5.78 μm without springs. The overall convergent-extension ratio of the 4-cell assembly is also smaller, down from 1.82 to 1.37, which is below all experimental observations. In particular, there is no improvement of the cell shape at the end of the simulation. Therefore, a passive elastic force on these connectors does not properly reproduce the effects of the surrounding tissue, which is spatially polarized and temporally stochastic, as all surrounding cells undergo similar, but randomized T1 and rosette processes as the unit in the middle. However, if we try to mimic the active spatio-temporal characteristics of the interaction with the surroundings, the model would essentially give us what we put in, and the whole exercise would become circular. The interaction with the neighboring cells depends on how the latter execute T1 or rosette transformation. Such transformations are what the model aims to predict, and thus should not be used as input to the model.

The ultimate solution is to compute a sufficiently large number of cells such that artificial boundary conditions imposed at the edges would not contaminate the dynamics within. This is a task envisioned for the near future. The present study strives to understand a simplified four-cell assembly undergoing T1 transition. Next, one should include a moderate number of cells and explore the dynamics of the rosettes, especially to answer these questions: What determines

which form, T1 or rosette, appears, and why? Does rosette formation involve the same or distinct pathways as in T1? Only then will we be ready to tackle a whole-tissue simulation.

D. Online movies

There are 4 online movies as described below:

SM.mov: the entire simulation comprising 3 stages: initial oscillation before onset of Shroom polarity ($t < 400$ s), AP edge contraction (400 s $< t <$ 822 s), and DV edge extension (822 s $< t <$ 1622 s). The shading within each cell indicates the medial myosin pulse, darker for higher medial myosin. The junctional myosin is indicated by the color spectrum.

SM1.mov: movie showing the stage of initial oscillation. The shading within each cell indicates the medial myosin pulse, darker for higher medial myosin. The junctional myosin is indicated by the color spectrum.

SM2.mov: movie showing the stage of AP edge contraction. The shading within each cell indicates the medial myosin pulse, darker for higher medial myosin. The junctional myosin is indicated by the color spectrum.

SM3.mov: movie showing the stage of DV edge extension. The shading within each cell indicates the medial myosin pulse, darker for higher medial myosin. The junctional myosin is indicated by the color spectrum.